SCIENCE CHINA
Information Sciences

• RESEARCH PAPER •

August 2021, Vol. 64 182311:1–182311:16
https://doi.org/10.1007/s11432-020-3139-9

Joint optimization of spectral efficiency for cell-free massive MIMO with network-assisted full duplexing

Xinjiang XIA[1,2], Pengcheng ZHU[1], Jiamin LI[1,2], Hao WU[3*], Dongming WANG[1,2*] & Yuanxue XIN[4]

[1]*National Mobile Communications Research Laboratory, Southeast University, Nanjing* 210096*, China;*
[2]*Purple Mountain Laboratories, Nanjing* 211111*, China;*
[3]*State Key Laboratory of Mobile Network and Mobile Multimedia Technology, Zhongxing Telecommunication Equipment Corporation, Shenzhen* 518055*, China;*
[4]*College of Internet of Things Engineering, Hohai University, Changzhou* 213022*, China*

Received 13 June 2020/Accepted 14 December 2020/Published online 8 July 2021

Abstract In this paper, we investigate duplex mode selection and transceiver design for cell-free massive multiple-input multiple-output (MIMO) with network-assisted full duplexing (NAFD), where the remote antenna units (RAUs) simultaneously serve both uplink and downlink users on the same time-frequency resource, and the joint transmission and reception are done at the central processing unit. We consider that each antenna can operate in three modes, i.e., uplink reception, downlink transmission and sleep. In particular, we model the problem as a mixed-integer optimization problem to maximize the aggregated spectral efficiency (SE) of downlinks and uplinks, where the quality-of-service constraints and power budget constraints are considered. Since the uplinks and downlinks are highly coupled, to address the design problem, we resolve the combinatorial problem by a series of nonconvex-convex approximate methods, such as equivalent formulations, iterative success convex approximations, and binary relaxations. In particular, a two-stage strategy is proposed to solve the optimization problem. In the first stage, we fix the mode selection vectors and then obtain the optimal transceivers with such a fairness strategy. In the second stage, with the transceiver parameters obtained from the first stage, we further optimize the duplex mode of each antenna. The algorithms of the two stages will alternately run in several loops until convergence. Numerical results indicate that the proposed solution can obtain SE performance that is close to the optimal exhaustive search solution and yields a higher SE gain compared with the traditional fixed-mode duplex scheme.

Keywords cell-free massive MIMO, network-assisted full duplexing, mode selection, success convex approximations, spectral efficiency.

Citation Xia X J, Zhu P C, Li J M, et al. Joint optimization of spectral efficiency for cell-free massive MIMO with network-assisted full duplexing. Sci China Inf Sci, 2021, 64(8): 182311, https://doi.org/10.1007/s11432-020-3139-9

1 Introduction

A dramatic increase in mobile devices and the high data-rate transmission in upcoming communication requires innovative technologies that make maximal use of spectrum resources. To improve network throughput, advanced techniques such as multiple-input multiple-output (MIMO) antennas and coordinated multipoint (CoMP) processes have been implemented in traditional wireless communication systems [1,2], where the user equipment and the base station (BS) operate in half-duplex transmission mode, such as time division duplex (TDD) and frequency division duplex (FDD), on a given frequency channel. To utilize radio resources more flexibly, flexible duplex techniques including dynamic TDD and flexible FDD have been supported by the fifth generation (5G) new radio as a key feature.

* Corresponding author (email: wu.hao89@zte.com.cn, wangdm@seu.edu.cn)

1.1 Related work

In the last decade, a powerful full-duplex technology, called co-frequency co-time full duplexing (CCFD), has been the focus of considerable attention by researchers [3–5]. By enabling simultaneous signal transmission and reception on the same time-frequency resource, theoretically, CCFD can double the spectral efficiency (SE) when compared with half-duplex [6–8]. However, in practical cellular systems with the CCFD BS, even when the self-interference of each CCFD BS could be suppressed to a very low level, the network performance is still limited by cross-link interference (CLI), that is, the interference from the transmitting antennas of one CCFD BS to the receiving antennas of another CCFD BS, and the interference from an uplink user to a downlink user.

Recently, a novel spatial domain duplexing has been proposed in [9], where one half-duplex BS serves a downlink user and another half-duplex BS serves an uplink user on the same time-frequency resources. Considering the channel hardening effect of large-scale distributed antennas, Refs. [10, 11] proposed a bidirectional dynamic network, which can also be considered as a spatial domain duplexing.

However, CLI is still a main challenge for CCFD networks and the spatial domain duplex techniques proposed in [9–11] as well as the flexible duplex of 5G new radio. To mitigate the negative effects of CLI, we should consider a new network architecture. Recently, cell-free massive MIMO has been an emerging technique to further improve the SE of wireless communication systems. From the aspect of the physical layer, cell-free massive MIMO can be considered as a single-cell large-scale distributed antenna system with joint processing [12]. From the aspect of network architecture, centralized networking makes cell-free massive MIMO have the capability of interference suppression.

The performance of CCFD cell-free massive MIMO systems was analyzed in [13], where the conclusion shows that the main limitation of the CCFD cell-free massive MIMO systems is the residual self-interference. In [14], a heap-based pilot assignment for CCFD cell-free massive MIMO with zero-forcing was investigated. Then, to achieve higher spectral and energy efficiencies, the authors in [15] proposed a jointly optimizing power control, remote antenna unit (RAU)-user association and RAU selection in a CCFD cell-free massive MIMO network. In [16, 17], to unified implementation of CCFD, flexible duplex, and CCFD cell-free massive MIMO, a network-assisted full duplex (NAFD) was proposed to mitigate the effect of CLI under cell-free architecture. Figure 1 shows a schematic diagram of the NAFD based on a cell-free massive MIMO. The uplink and downlink are simultaneously performed on the same time-frequency resource. Each RAU is connected to the central processing unit via a fronthaul link. The RAUs could be either with CCFD or half duplex. For the CCFD RAU, the transmit-receive self-interference of the RAU can be eliminated in the analog domain [18]. Therefore, we can treat the CCFD RAU as two RAUs, one for uplink reception and the other for downlink transmission. For NAFD, the downlink-to-uplink interference (including interferences between CCFD RAUs and interference between half-duplex RAUs) can be eliminated in the digital domain. Because the user terminal is usually unable to perform interference cancellation, uplink-to-downlink interference remains in the NAFD system. In [16], joint uplink-downlink user scheduling and user pairing has been proposed to reduce uplink-to-downlink interference.

With NAFD, one can choose the operating mode of uplink and downlink antennas dynamically adjusted as required to optimize the performance of the system. However, it is challenging work, as the uplink and downlink are highly coupled. Most of the existing studies on flexible duplex technologies assume the operating mode of uplink and downlink antennas is already given [19–21]. Nevertheless, some studies in the literature address antenna mode selection [15, 22, 23]. In [22], the authors proposed a transmit-receive antenna pair selection scheme for bidirectional CCFD communications, where each node is equipped with two antennas, used for transmission or reception. The work in [15] considers a half-array antenna mode selection and two-phase transmission, where the transmission time block is split into two phases, and uplink/downlink transmission modes can be independently selected by the two half-arrays of the antennas at the CCFD-enabled BS. In [23], the authors consider the problem of splitting uplink and downlink antennas of a BS in a CCFD cellular communication system, where the problem was modeled as a binary nonlinear optimization problem to minimize the sum of the mean squared error of the received data signals.

1.2 Motivations and contributions

Different from the previous studies, we aim to optimize duplex mode selection and transceiver design to maximize the SE of downlink users and uplink users under power and quality-of-service (QoS) constraints

in the NAFD scheme. Although the related studies in [16,17] studied an NAFD cell-free network, however, how to optimize the duplex mode is not considered, and the duplex mode is supposed to already be given. When the total number of antennas is limited, the traditional fixed mode duplex (such as CCFD and the bidirectional dynamic network) can effectively reduce the negative impact of CLI. However, as the number of RAUs or antennas per RAU increases, compared with flexible-mode duplex, the traditional fixed-mode duplex has a limited impact on CLI reduction. The reason behind is that, when the duplex mode is fixed, we have to try to reduce the CLI by optimizing the uplink power, downlink beamforming, and uplink receive. However, if the downlink/uplink channels or cross link channels are poor, there is a bottleneck in optimization. But for a flexible-mode duplex scheme, the CLI can be further reduced by flexibly changing the duplex mode of RAUs.

In summary, duplex mode selection supports the RAUs in finding better channel conditions and enabling the flexible transmission, which can significantly reduce the harmful effects of CLI and is benefit for achieving better system performance.

Hence, we optimize duplex mode selection for the NAFD scheme to further mitigate the negative effects of CLI and improve the sum of the SE of the downlink and uplink. In particular, we assume each antenna in the system can operate in three modes, i.e., uplink reception, downlink transmission and sleep, and introduce the integer assignment matrices to model the operational mode of antennas. As a result, the joint duplex mode selection, downlink beamforming design, uplink receiver design, and power control problem belong to the difficult class of mixed-integer nonconvex problems, where both types of binary and continuous variables, i.e., integer assignment matrices, transceivers vectors, and uplink power variables, are coupled with each other in the users' rate functions. To handle the highly coupled problem, we relax the binary constraints to logarithmic penalty functions and propose a two-stage strategy. Furthermore, as the continuous variables are still highly coupled together in each strategy, a series of nonconvex-convex approximate methods, such as equivalent formulations and iterative success convex approximations (SCAs) are used to decouple the variables. To our best knowledge, it is the first attempt to optimize duplex mode selection and transceiver design in cell-free massive MIMO with NAFD.

The contributions of this paper are summarized as follows:

• We study the SE maximization problem in NAFD under the constraints of QoS requirements of users, the operation mode of antennas and the transmit power of RAUs/users. This problem is practical but not yet investigated in the existing studies.

• A two-stage strategy of mode selection and transceiver design method is proposed to solve the SE maximization problem. Specifically, in the first stage, we fix the mode selection vectors and set each element of the vector as 0.5; then, we can obtain the optimal transceivers with such a fair strategy. In the second stage, with the transceivers obtained from the first stage, we further optimize the duplex mode selection. The algorithms of the two stages will be alternately run in several loops until convergence.

• To solve each subproblem of the two-stage optimization strategy, we propose two algorithms, where each has a series of nonconvex-convex approximate methods, such as equivalent formulations, iterative SCAs, and binary relaxations. Numerical results show that the proposed algorithm greatly improves the system performance over the conventional approaches, and it has fast convergence.

The remainder of this paper is organized as follows. Section 2 presents the channel mode and problem formulation. Then, we propose duplex mode selection and transceiver design algorithm for cell-free massive MIMO with NAFD in Section 3. In Section 4, the proposed algorithms of the two-stage optimization strategy are presented. The performance of the proposed algorithms is evaluated by simulations in Section 5. Finally, Section 6 summarizes the paper.

Notation. Throughout this paper, scalars are represented by lower-case letters (e.g., i), matrices are represented by upper-case bold letters (e.g., $\boldsymbol{H}$), and vectors are represented by lower-case bold letters (e.g., $\boldsymbol{v}$). The matrix inverse, conjugate transpose and l_p-norm of a vector are denoted $(.)^{-1}$, $(.)^{\mathrm{H}}$, and $|.|_p$ respectively. $\mathbb{C}^{M\times N}$ is used to denote the set of complex $M \times N$ matrices. The complex Gaussian distribution is represented by $\mathcal{CN}(.,.)$. Calligraphy letters are used to denote sets.

2 System model and problem formulation

2.1 Signal model

In this paper, we will investigate an NAFD network incorporating X RAUs equipped with M antennas,

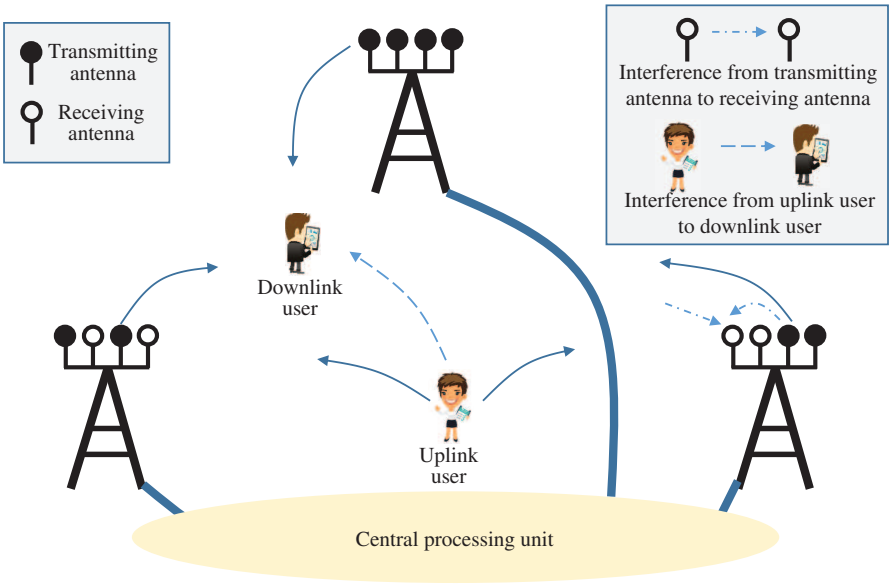

Figure 1 (Color online) Duplex mode selection of a cell-free with NAFD.

K single antenna downlink users and J single antenna uplink users, as shown in Figure 1, where IUI is the inter-user interference between downlink users and uplink users. In the figure, each uplink antenna in an RAU is subject to self-interference from the transmitting antennas of the RAU, and mutual-interference from the transmitting antennas of the other RAUs. Each antenna for RAUs in NAFD can operate in three modes, i.e., uplink reception, downlink transmission, and sleep. Theoretically, the hybrid duplex RAU could be considered as one transmitting RAU (T-RAU) and one receiving RAU (R-RAU). Therefore, we unify the self-interference and mutual-interference as inter-RAU interference (IRI). We let $\mathcal{K}=\{1,\ldots,K\}$, $\mathcal{J}=\{1,\ldots,J\}$, and $\mathcal{X}=\{1,\ldots,X\}$ represent the sets of downlink user indices, uplink user indices, and RAU indices, respectively. We initialize the mode of all the antennas and set each RAU as both a T-RAU and an R-RAU virtually.

For downlink, we assume that the RAUs employ linear transmit beamforming $\boldsymbol{w}_{\mathrm{D},k}=[\boldsymbol{w}_{\mathrm{D},1,k}^{\mathrm{T}},\ldots,\boldsymbol{w}_{\mathrm{D},X,k}^{\mathrm{T}}]^{\mathrm{T}}\in\mathbb{C}^{MX\times 1}$ to precode the data symbol $s_{\mathrm{D},k}\sim\mathcal{CN}(0,1)$ and cooperatively serve downlink user k. Then, the received signal at downlink user k can be expressed as

$$y_{\mathrm{D},k}=\boldsymbol{g}_{\mathrm{D},k}^{\mathrm{H}}\boldsymbol{w}_{\mathrm{D},k}s_{\mathrm{D},k}+\sum_{k'\neq k,k'\in\mathcal{K}}\boldsymbol{g}_{\mathrm{D},k}^{\mathrm{H}}\boldsymbol{w}_{\mathrm{D},k'}s_{\mathrm{D},k'}+\sum_{j\in\mathcal{J}}g_{\mathrm{IUI},j,k}\sqrt{P_{\mathrm{U},j}}s_{\mathrm{U},j}+n_{\mathrm{D},k},\tag{1}$$

where

$$\boldsymbol{g}_{\mathrm{D},k}=[\boldsymbol{g}_{\mathrm{D},1,k}^{\mathrm{T}},\boldsymbol{g}_{\mathrm{D},2,k}^{\mathrm{T}},\ldots,\boldsymbol{g}_{\mathrm{D},X,k}^{\mathrm{T}}]^{\mathrm{T}}\in\mathbb{C}^{MX\times 1}$$

is the channel vector between all T-RAUs and downlink user k, $s_{\mathrm{U},j}\sim\mathcal{CN}(0,1)$ represents the information signal sent for uplink user j, $n_{\mathrm{D},k}$ indicates the additive white Gaussian noise at the downlink user k satisfying $n_{\mathrm{D},k}\sim\mathcal{CN}(0,\sigma_{\mathrm{D},k}^2)$, $g_{\mathrm{IUI},j,k}$ denotes the channel coefficient from uplink user j to downlink user k, and $P_{\mathrm{U},j}$ is the transmit power of uplink user j.

Denote $\boldsymbol{G}_{\mathrm{IRI},x'}\in\mathbb{C}^{M\times MX}$ as the channel matrix from all T-RAUs to R-RAU x', i.e., the IRI channel from all T-RAUs to R-RAU x'. The baseband received signal at R-RAU x' is

$$\boldsymbol{y}_{\mathrm{U},x'}=\sum_{j\in\mathcal{J}}\boldsymbol{g}_{\mathrm{U},j,x'}\sqrt{P_{\mathrm{U},j}}s_{\mathrm{U},j}+\sum_{k\in\mathcal{K}}\boldsymbol{g}_{\mathrm{IRI},x'}\boldsymbol{w}_{\mathrm{D},k}s_{\mathrm{D},k}+\boldsymbol{n}_{\mathrm{U},x'},\tag{2}$$

where the vector $\boldsymbol{g}_{\mathrm{U},j,x'}\in\mathbb{C}^{M\times 1}$ denotes the channel from uplink user j to R-RAU x', $\boldsymbol{n}_{\mathrm{U},x'}\sim\mathcal{CN}(0,\sigma_{\mathrm{U},x'}^2\boldsymbol{I}_M)$ is the additive white Gaussian noise at R-RAU x'. The RAUs is assumed to collect the received signal $\boldsymbol{y}_{\mathrm{U},x'}$ and forward the signals to the central processing unit. Then, the received signal by central processing unit is given by

$$\boldsymbol{y}_{\mathrm{U}}=\sum_{j\in\mathcal{J}}\boldsymbol{g}_{\mathrm{U},j}\sqrt{P_{\mathrm{U},j}}s_{\mathrm{U},j}+\sum_{k\in\mathcal{K}}\boldsymbol{G}_{\mathrm{IRI}}\boldsymbol{w}_{\mathrm{D},k}s_{\mathrm{D},k}+\boldsymbol{n}_{\mathrm{U}},\tag{3}$$

where

$$\boldsymbol{g}_{\mathrm{U},j} = [\boldsymbol{g}_{\mathrm{U},j,1}^{\mathrm{T}}, \boldsymbol{g}_{\mathrm{U},j,2}^{\mathrm{T}}, \ldots, \boldsymbol{g}_{\mathrm{U},j,X}^{\mathrm{T}}]^{\mathrm{T}} \in \mathbb{C}^{MX\times 1},$$
$$\boldsymbol{G}_{\mathrm{IRI}} = [\boldsymbol{G}_{\mathrm{IRI},1}^{\mathrm{T}}, \boldsymbol{G}_{\mathrm{IRI},2}^{\mathrm{T}}, \ldots, \boldsymbol{G}_{\mathrm{IRI},X}^{\mathrm{T}}]^{\mathrm{T}} \in \mathbb{C}^{MX\times MX},$$

and

$$\boldsymbol{n}_{\mathrm{U}} = [\boldsymbol{n}_{\mathrm{U},1}^{\mathrm{T}}, \boldsymbol{n}_{\mathrm{U},2}^{\mathrm{T}}, \ldots, \boldsymbol{n}_{\mathrm{U},X}^{\mathrm{T}}]^{\mathrm{T}} \in \mathbb{C}^{MX\times 1}.$$

In practice, we assume the channel state information (CSI) between R-RAUs and T-RAUs (all $\boldsymbol{G}_{\mathrm{IRI},x,x'}$) is imperfect due to the channel estimation errors. Specifically, we model the inter-RAU channel $\boldsymbol{g}_{\mathrm{IRI},x,x'}$ as

$$\boldsymbol{G}_{\mathrm{IRI},x,x'} = \hat{\boldsymbol{G}}_{\mathrm{IRI},x,x'} + \tilde{\boldsymbol{G}}_{\mathrm{IRI},x,x'},$$

where $\hat{\boldsymbol{G}}_{\mathrm{IRI},x,x'}$ denotes the estimated channel and $\tilde{\boldsymbol{G}}_{\mathrm{IRI},x,x'}$ denotes the channel estimation error. It is assumed that the elements of $\tilde{\boldsymbol{G}}_{\mathrm{IRI},x,x'}$ follow a independent identically distributed (i.i.d.) Gaussian distribution, i.e.,

$$\mathrm{vec}(\tilde{\boldsymbol{G}}_{\mathrm{IRI},x,x'}) \sim \mathcal{CN}(\boldsymbol{0}, \delta_{\mathrm{IRI},x,x'}^2 \boldsymbol{I}_{M^2}),$$

where $\boldsymbol{I}_{M^2}$ denotes an $M^2\times M^2$ identity matrix, and $\delta_{\mathrm{IRI},x,x'}^2$ denotes the residual error gain; for simplicity. We further assume $\delta_{\mathrm{IRI},x,x'}^2 = \delta_{\mathrm{IRI}}^2, \forall x, x'$.

Due to the channel estimation errors, the received signal at the central processing unit can be modeled as follows:

$$\hat{\boldsymbol{y}}_{\mathrm{U}} = \sum_{j\in\mathcal{J}} \boldsymbol{g}_{\mathrm{U},j}\sqrt{P_{\mathrm{U},j}}s_{\mathrm{U},j} + \sum_{k\in\mathcal{K}} \tilde{\boldsymbol{G}}_{\mathrm{IRI}}\boldsymbol{w}_{\mathrm{D},k}s_{\mathrm{D},k} + \boldsymbol{n}_{\mathrm{U}}, \tag{4}$$

where

$$\tilde{\boldsymbol{G}}_{\mathrm{IRI}} = [\tilde{\boldsymbol{G}}_{\mathrm{IRI},1}^{\mathrm{T}}, \tilde{\boldsymbol{G}}_{\mathrm{IRI},2}^{\mathrm{T}}, \ldots, \tilde{\boldsymbol{G}}_{\mathrm{IRI},X}^{\mathrm{T}}]^{\mathrm{T}},$$

and we can further obtain the covariance matrix of IRI between R-RAU x' and T-RAU x as

$$\mathbb{E}[\tilde{\boldsymbol{G}}_{\mathrm{IRI},x,x'}\boldsymbol{w}_{\mathrm{D},x,k}\boldsymbol{w}_{\mathrm{D},x,k}^{\mathrm{H}}\tilde{\boldsymbol{G}}_{\mathrm{IRI},x,x'}^{\mathrm{H}}] = \delta_{\mathrm{IRI}}^2\|\boldsymbol{w}_{\mathrm{D},x,k}\|^2\boldsymbol{I}_M. \tag{5}$$

2.2 Signal model of NAFD with duplex mode selection

As illustrated in Figure 1, M antennas at the RAUs may transmit and receive, however, the direction in receive mode or transmit mode needs to be selected. To determine which mode each antenna should operate in, we define two binary assignment vectors, $\boldsymbol{q}_{\mathrm{D},x}, \boldsymbol{q}_{\mathrm{U},x'} \in \{0,1\}^{M\times 1}$, for the transmit mode and receive mode, respectively, such that $q_{\mathrm{D},x,m}(q_{\mathrm{U},x',m'})$ is equal to 1 if antenna $m(m')$ is operating in transmit mode (receive mode). Furthermore, if both $q_{\mathrm{D},x,m}$ and $q_{\mathrm{U},x,m}$ are equal to 0, the antenna m is set to sleep mode. Then, we have $\boldsymbol{q}_{\mathrm{D}} = [\boldsymbol{q}_{\mathrm{D},1}, \boldsymbol{q}_{\mathrm{D},2}, \ldots, \boldsymbol{q}_{\mathrm{D},X}] \in \{0,1\}^{MX\times 1}$, $\boldsymbol{q}_{\mathrm{U}} = [\boldsymbol{q}_{\mathrm{U},1}, \boldsymbol{q}_{\mathrm{U},2}, \ldots, \boldsymbol{q}_{\mathrm{U},X}] \in \{0,1\}^{MX\times 1}$. To further clarify the relationship of assignment between $\boldsymbol{q}_{\mathrm{D}}$ and $\boldsymbol{q}_{\mathrm{U}}$, we transform the assignment vectors into diagonal assignment matrices, such that $\boldsymbol{Q}_{\mathrm{D}} = \mathrm{diag}(\boldsymbol{q}_{\mathrm{D}})$ and $\boldsymbol{Q}_{\mathrm{U}} = \mathrm{diag}(\boldsymbol{q}_{\mathrm{U}})$.

Then, the effective received signal of $\bar{y}_{\mathrm{D},k}$ and the detected received signal $\bar{y}_{\mathrm{U},j}$ can be rewritten in a compact form as

$$\bar{y}_{\mathrm{U},j} = \bar{\boldsymbol{u}}_{\mathrm{U},j}^{\mathrm{H}}\hat{\boldsymbol{y}}_{\mathrm{U}} = \bar{\boldsymbol{u}}_{\mathrm{U},j}^{\mathrm{H}}\sum_{j\in\mathcal{J}}\boldsymbol{g}_{\mathrm{U},j}\sqrt{P_{\mathrm{U},j}}s_{\mathrm{U},j} + \bar{\boldsymbol{u}}_{\mathrm{U},j}^{\mathrm{H}}\sum_{k\in\mathcal{K}}\boldsymbol{G}_{\mathrm{IRI}}\bar{\boldsymbol{w}}_{\mathrm{D},k}s_{\mathrm{D},k} + \bar{\boldsymbol{u}}_{\mathrm{U},j}^{\mathrm{H}}\boldsymbol{n}_{\mathrm{U}}, \tag{6a}$$

$$\bar{y}_{\mathrm{D},k} = \boldsymbol{g}_{\mathrm{D},k}^{\mathrm{H}}\bar{\boldsymbol{w}}_{\mathrm{D},k}s_{\mathrm{D},k} + \sum_{k'\neq k,k\in\mathcal{K}}\boldsymbol{h}_{\mathrm{D},k}^{\mathrm{H}}\bar{\boldsymbol{w}}_{\mathrm{D},k'}s_{\mathrm{D},k'} + \sum_{j\in\mathcal{J}}g_{\mathrm{IUI},j,k}\sqrt{P_{\mathrm{U},j}}s_{\mathrm{U},j} + n_{\mathrm{D},k}, \tag{6b}$$

where

$$\bar{\boldsymbol{w}}_{\mathrm{D},k} = \boldsymbol{Q}_{\mathrm{D}}\boldsymbol{w}_{\mathrm{D},k} = [\bar{\boldsymbol{w}}_{\mathrm{D},1,k}^{\mathrm{T}}, \ldots, \bar{\boldsymbol{w}}_{\mathrm{D},X,k}^{\mathrm{T}}]^{\mathrm{T}} \in \mathbb{C}^{MX\times 1}$$

represents the effective beamforming vector and

$$\bar{\boldsymbol{u}}_{\mathrm{U},j} = \boldsymbol{Q}_{\mathrm{U}}\boldsymbol{u}_{\mathrm{U},j} = [\bar{\boldsymbol{u}}_{\mathrm{U},1,j}^{\mathrm{T}}, \bar{\boldsymbol{u}}_{\mathrm{U},2,j}^{\mathrm{T}}, \ldots, \bar{\boldsymbol{u}}_{\mathrm{U},X,j}^{\mathrm{T}}]^{\mathrm{T}} \in \mathbb{C}^{MX\times 1}$$

represents the effective receiver vector, $\boldsymbol{u}_{\mathrm{U},j}$ is the corresponding receiver vector.

It is clear that the value of the effective received signal of downlink user k depends on the effective beamforming design of the downlink. When $q_{\mathrm{D},x,m} = 1$, the corresponding $\bar{w}_{\mathrm{D},x,m,k} = w_{\mathrm{D},x,m,k}$, which means that the antenna m is set to transmit mode; in contrast, the corresponding $\bar{u}_{\mathrm{U},x,m,j} = u_{\mathrm{U},x,m,j}$, which means that the antenna m is set to receive mode.

Then, we can write the signal-to-interference-plus-noise ratios (SINR) of downlink user k as

$$r_{\mathrm{D},k} = \frac{|\boldsymbol{g}_{\mathrm{D},k}^{\mathrm{H}} \bar{\boldsymbol{w}}_{\mathrm{D},k}|^2}{\gamma_{\mathrm{D},k}}, \tag{7}$$

where

$$\gamma_{\mathrm{D},k} = \sum_{k' \neq k, k' \in \mathcal{K}} |\boldsymbol{g}_{\mathrm{D},k}^{\mathrm{H}} \bar{\boldsymbol{w}}_{\mathrm{D},k'}|^2 + \sum_{j \in \mathcal{J}} P_{\mathrm{U},j} |g_{\mathrm{IUI},j,k}|^2 + \sigma_{\mathrm{D},k}^2. \tag{8}$$

As we can see, by optimizing the downlink beamforming vectors for T-RAUs and the transmission power of uplink users, the NAFD system can reduce the interference from uplink users and further improve the downlink performance.

Then, the SINR for each uplink user j can be expressed as

$$r_{\mathrm{U},j} = \frac{P_{\mathrm{U},j} |\bar{\boldsymbol{u}}_{\mathrm{U},j}^{\mathrm{H}} \boldsymbol{g}_{\mathrm{U},j}|^2}{\gamma_{\mathrm{U},j}}, \tag{9}$$

where

$$\gamma_{\mathrm{U},j} = \sum_{j' \neq j, j' \in \mathcal{J}} P_{\mathrm{U},j'} |\bar{\boldsymbol{u}}_{\mathrm{U},j}^{\mathrm{H}} \boldsymbol{g}_{\mathrm{U},j'}|^2 + \sum_{x' \in \mathcal{X}} \sigma_{\mathrm{U},x'}^2 \|\bar{\boldsymbol{u}}_{\mathrm{U},x',j}\|^2 + \sum_{k \in \mathcal{K}} \|\bar{\boldsymbol{w}}_{\mathrm{D},k}\|^2 \delta_{\mathrm{IRI}}^2 \|\bar{\boldsymbol{u}}_{\mathrm{U},j}\|^2 \tag{10}$$

is the power of interference-plus-noise for the uplink user j,

2.3 Problem formulation

We aim to jointly optimize $\{P_{\mathrm{U},j}, \boldsymbol{u}_{\mathrm{U},j,x'}, \boldsymbol{w}_{\mathrm{D},k}, q_{\mathrm{D},x,m}, q_{\mathrm{U},x',m'}\} \forall k, x, x', j$ to maximize the SE problem under power and QoS constraints. Mathematically, the design problem is

$$\max_{\{\boldsymbol{q}_{\mathrm{D}}, \boldsymbol{q}_{\mathrm{U}}, \boldsymbol{w}_{\mathrm{D},k}, \boldsymbol{u}_{\mathrm{U},j}, P_{\mathrm{U},j}\}} \sum_{k \in \mathcal{K}} \ln(1 + r_{\mathrm{D},k}) + \sum_{j \in \mathcal{J}} \ln(1 + r_{\mathrm{U},j}) = \sum_{k \in \mathcal{K}} R_{\mathrm{D},k} + \sum_{j \in \mathcal{J}} R_{\mathrm{U},j} \tag{11a}$$

$$\text{s.t.} \quad \sum_{k \in \mathcal{K}} \|\boldsymbol{Q}_{\mathrm{D},x} \boldsymbol{w}_{\mathrm{D},x,k}\|^2 \leqslant P_{\mathrm{D},x}, \ \forall x, \tag{11b}$$

$$p_{\mathrm{U},j} \leqslant P_{\mathrm{U},j}, \ \forall j, \tag{11c}$$

$$q_{\mathrm{D},x,m}, q_{\mathrm{U},x',m'} \in \{0,1\}, \ \forall x, x', m, m', \tag{11d}$$

$$q_{\mathrm{D},x,m} + q_{\mathrm{U},x,m} \in \{0,1\}, \ \forall x, m, \tag{11e}$$

$$r_{\mathrm{D},k} \geqslant r_{\mathrm{D},\min,k}, \ \forall k, \tag{11f}$$

$$r_{\mathrm{U},j} \geqslant r_{\mathrm{U},\min,j}, \ \forall j, \tag{11g}$$

where $P_{\mathrm{D},x}$, $P_{\mathrm{U},j}$, (11b), and (11c) are the power consumption budget for T-RAU x, uplink user j and power constraints for T-RAU x, uplink user j, respectively. Eqs. (11f) and (11g) are the QoS constraints for downlink user k and uplink user j, respectively. The conditions (11d) and (11e) impose that binary assignment vectors $q_{\mathrm{D},x,m}$ and $q_{\mathrm{U},x',m'}$ of each antenna should be either 0 or 1. Moreover, when the both $q_{\mathrm{D},x,m}$ and $q_{\mathrm{U},x',m}$ are equal to zero, the antenna operates in sleep mode.

3 Duplex mode selection and transceiver design

Note that the optimization problem (11) is a mixed-integer problem and is NP-hard [24]. Since there is a finite set of possible solutions, one can simply search all solutions, i.e., perform an exhaustive search solution (EXH). However, if we do so, we might have to perform up to $O(3^{MX})$ optimization subproblems to find the optimal solution. Hence, as an alternative solution to the combinatorial problem (11), we relax the binary variable $\boldsymbol{q}_{\mathrm{D}}, \boldsymbol{q}_{\mathrm{U}} \in \{0,1\}$ by a linear constraint as $\boldsymbol{q}_{\mathrm{D}}, \boldsymbol{q}_{\mathrm{U}} \in [0,1]$ in order to find a low-complexity formulation. In practice, we regularize the objective function with a penalty term as in [25–28], and obtain an approximate solution with a regularization term for (11) as

$$\max_{\{\boldsymbol{q}_{\mathrm{D}}, \boldsymbol{q}_{\mathrm{U}}, \boldsymbol{w}_{\mathrm{D},k}, \boldsymbol{u}_{\mathrm{U},j}, P_{\mathrm{U},j}\}} \sum_{k \in \mathcal{K}} R_{\mathrm{D},k} + \sum_{j \in \mathcal{J}} R_{\mathrm{U},j} - f(q_{\mathrm{D},x,m}, q_{\mathrm{U},x',m'}) \tag{12a}$$

$$\text{s.t. } 0 \leqslant q_{\mathrm{D},x,m} \leqslant 1,\ \forall x, m, \tag{12b}$$

$$0 \leqslant q_{\mathrm{U},x',m'} \leqslant 1,\ \forall x', m', \tag{12c}$$

$$0 \leqslant q_{\mathrm{D},x,m} + q_{\mathrm{U},x,m} \leqslant 1,\ \forall x, m, \tag{12d}$$

$$(11\mathrm{b}),\ (11\mathrm{c}),\ (11\mathrm{f}),\ (11\mathrm{g}), \tag{12e}$$

where $f(q_{\mathrm{D},x,m}, q_{\mathrm{U},x',m'})$ is a penalty function to encouraging discrete-value solutions (i.e., 0 and 1) for $q_{\mathrm{D},x,m}$ and $q_{\mathrm{U},x',m'}$. Due to the above relax operation, the binary outcome for the solution of $q_{\mathrm{D},x,m}$ and $q_{\mathrm{U},x',m'}$ cannot be guaranteed; therefore, Eq. (12) can only be considered as an approximate problem for (11) but not an equivalent formulation. After solving (12) with the discrete-value penalty function, if $q_{\mathrm{D},x,m}, q_{\mathrm{U},x',m'} \in \{0,1\}$, the solution of (12) is straightforwardly a feasible solution of (11). Furthermore, if $q_{\mathrm{D},x,m}, q_{\mathrm{U},x',m'} \notin \{0,1\}$, the feasible point for (11) can be found by setting the conditions as follows:

$$q_{\mathrm{D},x,m}, q_{\mathrm{U},x',m'} = \begin{cases} 1, & q_{\mathrm{D},x,m}, q_{\mathrm{U},x',m'} \geqslant \varphi, \\ 0, & \text{otherwise}, \end{cases} \tag{13}$$

where φ is a predefined threshold. Thus, the solution found by solving (12) can be used to obtain a feasible point for the original problem (11).

The method to promote the binary solution for variables $q_{\mathrm{D},x,m}$ and $q_{\mathrm{U},x',m'}$ is the well-known sparsity-inducing penalty function proposed in [26, 29], as given by

$$\begin{aligned} f\left(q_{\mathrm{D},x,m}, q_{\mathrm{U},x',m'}\right) = &\sum_{x\in\mathcal{X}} \sum_{m\in\mathcal{M}_{\mathrm{D},x}} \left(\log\left(q_{\mathrm{D},x,m} + \varepsilon\right) + \log\left(\left(1 - q_{\mathrm{D},x,m}\right) + \varepsilon\right)\right) \\ &+ \sum_{x'\in\mathcal{X}} \sum_{m'\in\mathcal{M}_{\mathrm{U},x'}} \left(\log\left(q_{\mathrm{U},x',m'} + \varepsilon\right) + \log\left(\left(1 - q_{\mathrm{U},x',m'}\right) + \varepsilon\right)\right), \end{aligned} \tag{14}$$

where $\varepsilon \geqslant 0$, $\mathcal{M}_{\mathrm{D},x}$, and $\mathcal{M}_{\mathrm{U},x'}$ are small positive constants used to limit the dynamic range of the log function, the sets of antennas for T-RAU x and the sets of antennas for R-RAU x', respectively. The use of the log in (14) is justified by the fact that, when $q_{\mathrm{U},x,m}, q_{\mathrm{D},x',m'} = \{0,1\}$, we can obtain [25]

$$q_{\mathrm{D},x,m}\left(1 - q_{\mathrm{D},x,m}\right) = 0, \quad q_{\mathrm{U},x',m'}\left(1 - q_{\mathrm{U},x',m'}\right) = 0. \tag{15}$$

Furthermore, the logarithmic penalty function in (14) is used to smooth (15) in order to obtain an exact penalty optimization approach for the original mixed-integer programming problem [29].

Although problem (11) can be approximated by problem (12), the solution is still not easy to obtain because the $\boldsymbol{Q}_{\mathrm{D}}$, $\boldsymbol{w}_{\mathrm{D},k}$, $\boldsymbol{Q}_{\mathrm{U}}$, and $\boldsymbol{u}_{\mathrm{U},j}$ are tightly coupled in both the objective function and the constraints.

To solve the coupled problem, we propose an iterative SCA-based algorithm. The main idea of the proposed algorithm is that in stage I, when fixing the $\boldsymbol{q}_{\mathrm{D},x}$ and $\boldsymbol{q}_{\mathrm{U},x'}$ and setting $q_{\mathrm{D},x,m} = q_{\mathrm{U},x',m'} = 0.5$, $\forall x, x', m, m'$, we can find optimal transceivers by solving the original problem (12) with the SCA method. Then, in stage II, when fixing the transceivers obtained from stage I, we can obtain the operation mode of RAUs.

The main reason can be summarized as follows. In stage I, since $q_{\mathrm{D},x,m}$ and $q_{\mathrm{U},x',m'}$ are both set to 0.5, the transceivers that we obtained are based on a fairness strategy, i.e., the SE gains obtained are mainly dependent on the CSI; if the downlink CSI gain between the antenna m and downlink users is better than the uplink CSI gain between the antenna m and uplink users, then the SE gains of the downlink will have the greatest probability of being higher than those of the uplink. As a result, the downlink transmitting antenna m should be more effective than the uplink receiving antenna m. Furthermore, in stage II, when the transceivers are fixed, the result of mode selection mainly relies on the SE gains obtained by users. That is, if the SE gains obtained by downlink users will be more effective than those of uplink users, the antenna m should operate in the downlink mode; in contrast, the antenna m should operate in the uplink mode. Furthermore, if the SE gains obtained by downlink/uplink users will be no than zero, the antenna m should operate in sleep mode.

To summarize, based on the above analysis, we propose the overall mode selection and transceiver design algorithm as shown in Algorithm 1.

Algorithm 1 Duplex mode selection and transceiver design algorithm

Input: Initialization: $\boldsymbol{q}_{\mathrm{D}}^{(0)}$, $\boldsymbol{q}_{\mathrm{U}}^{(0)}$, $\boldsymbol{w}_{\mathrm{D},k}^{(0)}$, $\boldsymbol{u}_{\mathrm{U},j}^{(0)}$, $P_{\mathrm{U},j}^{(0)}$.
Set $\boldsymbol{q}_{\mathrm{D}}^{(0)}, \boldsymbol{q}_{\mathrm{U}}^{(0)} \to \{0.5\}^{MX\times 1}$, loop $\to 0$.
repeat
  Fix $\boldsymbol{Q}_{\mathrm{D}}^{(n)}$, $\boldsymbol{Q}_{\mathrm{U}}^{(n)}$, solve problem (12) and obtain optimal transceivers $\boldsymbol{w}_{\mathrm{D},k}^{\dagger}$, $\boldsymbol{u}_{\mathrm{U},j}^{\dagger}$, $P_{\mathrm{U},j}^{\dagger}$ by Algorithm 2 in Subsection 4.1;
  Update $\boldsymbol{w}_{\mathrm{D},k}^{(n)} \to \boldsymbol{w}_{\mathrm{D},k}^{\dagger}$; $\boldsymbol{u}_{\mathrm{U},j}^{(n)} \to \boldsymbol{u}_{\mathrm{U},j}^{\dagger}$; $P_{\mathrm{U},j}^{(n)} \to P_{\mathrm{U},j}^{\dagger}$;
  Fix $\boldsymbol{w}_{\mathrm{D},k}^{(n)}$, $\boldsymbol{u}_{\mathrm{U},j}^{(n)}$, $P_{\mathrm{U},j}^{(n)}$, solve problem (12) and obtain the result of duplex mode selection $\{\boldsymbol{Q}_{\mathrm{D}}^{\dagger}, \boldsymbol{Q}_{\mathrm{U}}^{\dagger}\}$ by Algorithm 3 in Subsection 4.2;
  Update $\boldsymbol{Q}_{\mathrm{D}}^{(n+1)} \to \boldsymbol{Q}_{\mathrm{D}}^{\dagger}$; $\boldsymbol{Q}_{\mathrm{U}}^{(n+1)} \to \boldsymbol{Q}_{\mathrm{U}}^{\dagger}$;
until convergence;
return the optimal solutions $\{P_{\mathrm{U},j}^{\dagger}, \boldsymbol{W}_{\mathrm{D},k}^{\dagger}, \boldsymbol{u}_{\mathrm{U},j}^{\dagger}, \boldsymbol{Q}_{\mathrm{D}}^{\dagger}, \boldsymbol{Q}_{\mathrm{U}}^{\dagger}\}$.

4 Two-stage optimization strategy for duplex mode selection and transceiver design

In this section, we provide a two-stage optimization strategy for duplex mode selection and transceiver design of problem (12). Specifically, in stage I, we set $q_{\mathrm{D},x,m}^{(0)}, q_{\mathrm{U},x',m'}^{(0)} \to 0.5, \forall x, x', m, m'$ and optimize the downlink beamforming, uplink receiver, and uplink transceiver. In stage II, by fixing $\{\boldsymbol{w}_{\mathrm{D},k}, \boldsymbol{u}_{\mathrm{U},j}, P_{\mathrm{U},j}\}$ obtained in stage I, we optimize the duplex mode selection.

4.1 Stage I: solution for problem (12) with fixed duplex mode.

It is obvious that if the $\boldsymbol{q}_{\mathrm{D},x}$ and $\boldsymbol{q}_{\mathrm{U},x'}$ are fixed, the problem (12) can be rewritten as

$$\begin{aligned}&\max_{\{\boldsymbol{w}_{\mathrm{D},k},\boldsymbol{u}_{\mathrm{U},j},P_{\mathrm{U},j}\}} \sum_{k\in\mathcal{K}} R_{\mathrm{D},k} + \sum_{j\in\mathcal{J}} R_{\mathrm{U},j} - f(q_{\mathrm{D},x,m}^{(0)}, q_{\mathrm{U},x',m'}^{(0)})\\ &\text{s.t.}\quad \text{(11b)},\ \text{(11c)},\ \text{(11f)},\ \text{(11g)},\end{aligned} \tag{16}$$

with $\boldsymbol{q}_{\mathrm{D}} = \boldsymbol{q}_{\mathrm{D}}^{(0)}$ and $\boldsymbol{q}_{\mathrm{U}} = \boldsymbol{q}_{\mathrm{U}}^{(0)}$.

We can find that problem (16) is a nonconvex problem due to the nonconvex object and the constraints (11f) and (11g). In what follows, we show how to address the complicated nonconvex object and the constraints (11f) and (11g) of problem (16) in order.

To proceed, motivated by [30], we can obtain the following inequalities:

$$\ln\left(1+\frac{|b|^2}{a}\right) \geqslant Z(a,b,a^{(n)},b^{(n)}) = \ln\left(1+\frac{|b^{(n)}|^2}{a^{(n)}}\right) - \frac{|b^{(n)}|^2}{a^{(n)}} + 2\frac{\mathrm{Re}\{b^{(n)}b\}}{a^{(n)}} - \frac{|b^{(n)}|^2(|b|^2+a)}{a^{(n)}(a^{(n)}+|b^{(n)}|^2)}, \tag{17a}$$

$$\frac{\boldsymbol{b}^{\mathrm{H}}\boldsymbol{A}\boldsymbol{b}}{a} \geqslant \bar{Z}(a,\boldsymbol{b},a^{(n)},\boldsymbol{b}^{(n)},\boldsymbol{A}) = \frac{2\Re\{(\boldsymbol{b}^{(n)})^{\mathrm{H}}\boldsymbol{A}\boldsymbol{b}\}}{a^{(n)}} - \frac{(\boldsymbol{b}^{(n)})^{\mathrm{H}}\boldsymbol{A}\boldsymbol{b}^{(n)}a}{\left(a^{(n)}\right)^2}, \tag{17b}$$

$$\boldsymbol{b}^{\mathrm{H}}\boldsymbol{A}\boldsymbol{b} \geqslant \hat{Z}(\boldsymbol{b},\boldsymbol{b}^{(n)},\boldsymbol{A}) = (\boldsymbol{b}^{(n)})^{\mathrm{H}}\boldsymbol{A}\boldsymbol{b}^{(n)} + 2\Re\{(\boldsymbol{b}^{(n)})^{\mathrm{H}}\boldsymbol{A}(\boldsymbol{b}-\boldsymbol{b}^{(n)})\}, \tag{17c}$$

where $a>0$, $b>0$, $\ln(1+\frac{|b^{(n)}|^2}{a^{(n)}}) - \frac{|b^{(n)}|^2}{a^{(n)}} < 0$.

Let us treat the nonconcave object of (16) first. As observed in [31], by introducing a set of auxiliary variables $\{\lambda_{\mathrm{D},k}\}$, Eq. (7) can be approximated by

$$r_{\mathrm{D},k} \geqslant \frac{\lambda_{\mathrm{D},k}^2}{\gamma_{\mathrm{D},k}}, \tag{18}$$

where

$$|\boldsymbol{g}_{\mathrm{D},k}^{\mathrm{H}}\boldsymbol{Q}_{\mathrm{D}}^{(0)}\boldsymbol{w}_{\mathrm{D},k}|^2 \geqslant \lambda_{\mathrm{D},k}^2 \tag{19}$$

with the linear constraint as

$$\lambda_{\mathrm{D},k} \geqslant 0. \tag{20}$$

As a result, given a feasible point $(\boldsymbol{w}_{\mathrm{D},k}^{(n)}, P_{\mathrm{U},j}^{(n)}, \lambda_{\mathrm{D},k}^{(n)})$, $R_{\mathrm{D},k}$ is lower-bounded by

$$\ln(1+r_{\mathrm{D},k}) \geqslant Z(\gamma_{\mathrm{D},k}, \lambda_{\mathrm{D},k}, \gamma_{\mathrm{D},k}^{(n)}, \lambda_{\mathrm{D},k}^{(n)}), \tag{21}$$

and nonconvex constraint (19) can be transformed into

$$\hat{Z}(\boldsymbol{Q}_{\mathrm{D}}^{(0)}\boldsymbol{w}_{\mathrm{D},k}, \boldsymbol{Q}_{\mathrm{D}}^{(0)}\boldsymbol{w}_{\mathrm{D},k}^{(n)}, \boldsymbol{G}_{\mathrm{D},k}) \geqslant \lambda_{\mathrm{D},k}^2, \tag{22}$$

where $\boldsymbol{G}_{\mathrm{D},k} = \boldsymbol{g}_{\mathrm{D},k}\boldsymbol{g}_{\mathrm{D},k}^{\mathrm{H}}$. Note that to arrive at (22), we have used the equality $|\boldsymbol{c}^{\mathrm{H}}\boldsymbol{d}|^2 = \boldsymbol{d}^{\mathrm{H}}\boldsymbol{C}\boldsymbol{d}$, where $C = \boldsymbol{c}\boldsymbol{c}^{\mathrm{H}}$. Further, we have the constraint (22) according to (17c).

Then, we try to address (9) in the objective function. Since the variables in (9) are highly coupled, we first approximate (9) with the SCA method. By introducing a series of variables $\{\alpha_{\mathrm{D}}\}$, $\{t_{\mathrm{DU},j}\}$, $\{\eta_{\mathrm{U},j,j'}\}$, $\{\beta_{\mathrm{U},j}\}$, we can obtain

$$\sum_{k\in\mathcal{K}} \|\boldsymbol{Q}_{\mathrm{D}}^{(0)}\boldsymbol{w}_{\mathrm{D},k}\|^2 \leqslant \alpha_{\mathrm{D}}, \tag{23a}$$

$$\alpha_{\mathrm{D}}\|\boldsymbol{Q}_{\mathrm{U}}^{(0)}\boldsymbol{u}_{\mathrm{U},j}\|^2 \leqslant t_{\mathrm{DU},j}^2, \tag{23b}$$

$$P_{\mathrm{U},j'}|\boldsymbol{u}_{\mathrm{U},j}^{\mathrm{H}}\boldsymbol{Q}_{\mathrm{U}}^{(0)}\boldsymbol{g}_{\mathrm{U},j'}|^2 \leqslant \eta_{\mathrm{U},j,j'}^2, \tag{23c}$$

$$P_{\mathrm{U},j}|\boldsymbol{u}_{\mathrm{U},j}^{\mathrm{H}}\boldsymbol{Q}_{\mathrm{U}}^{(0)}\boldsymbol{g}_{\mathrm{U},j}|^2 \geqslant \beta_{\mathrm{U},j}^2. \tag{23d}$$

It is obvious that constraint (23a) is a convex second-order cone (SOC) constraint. However, constraints (23b)–(23d) are nonconvex. Further resorting to the constraints (23b)–(23d), we can obtain

$$\|\boldsymbol{Q}_{\mathrm{U}}^{(0)}\boldsymbol{u}_{\mathrm{U},j}\|^2 \leqslant \frac{t_{\mathrm{DU},j}^2}{\alpha_{\mathrm{D}}}, \tag{24a}$$

$$|\boldsymbol{u}_{\mathrm{U},j}^{\mathrm{H}}\boldsymbol{Q}_{\mathrm{U}}^{(0)}\boldsymbol{g}_{\mathrm{U},j'}|^2 \leqslant \frac{\eta_{\mathrm{U},j,j'}^2}{P_{\mathrm{U},j'}}, \tag{24b}$$

$$|\boldsymbol{u}_{\mathrm{U},j}^{\mathrm{H}}\boldsymbol{Q}_{\mathrm{U}}^{(0)}\boldsymbol{g}_{\mathrm{U},j}|^2 \geqslant \frac{\beta_{\mathrm{U},j}^2}{P_{\mathrm{U},j}}. \tag{24c}$$

We can see that all the inequations in (24) are still nonconvex. By applying (17b) and (17c), Eq. (24) can be bounded by

$$\|\boldsymbol{Q}_{\mathrm{U}}^{(0)}\boldsymbol{u}_{\mathrm{U},j}\|^2 \leqslant \bar{Z}\big(\alpha_{\mathrm{D}}, t_{\mathrm{DU},j}, \alpha_{\mathrm{D}}^{(n)}, t_{\mathrm{DU},j}^{(n)}, 1\big), \tag{25a}$$

$$|\boldsymbol{u}_{\mathrm{U},j}^{\mathrm{H}}\boldsymbol{Q}_{\mathrm{U}}^{(0)}\boldsymbol{g}_{\mathrm{U},j'}|^2 \leqslant \bar{Z}\big(P_{\mathrm{U},j'}, \eta_{\mathrm{U},j,j'}, P_{\mathrm{U},j'}^{(n)}, \eta_{\mathrm{U},j,j'}^{(n)}, 1\big), \tag{25b}$$

$$\hat{Z}\big(\boldsymbol{u}_{\mathrm{U},j}, \boldsymbol{u}_{\mathrm{U},j}^{(n)}, \boldsymbol{g}_{\mathrm{U},j}\big) \geqslant \frac{\beta_{\mathrm{U},j}^2}{P_{\mathrm{U},j}}. \tag{25c}$$

As a result, Eq. (9) can be approximated by

$$\bar{r}_{\mathrm{U},j} \geqslant \frac{\beta_{\mathrm{U},j}^2}{\bar{\gamma}_{\mathrm{U},j}} \tag{26}$$

with the linear constraint as

$$\beta_{\mathrm{U},j} \geqslant 0, \tag{27}$$

and where

$$\bar{\gamma}_{\mathrm{U},j} = \eta_{\mathrm{U},j,j'}^2 + \delta_{\mathrm{IRI}}^2 t_{\mathrm{DU},j}^2 + \sum_{x'\in\mathcal{X}} \sigma_{\mathrm{U},x'}^2 \|\boldsymbol{Q}_{\mathrm{U}}^{(0)}\boldsymbol{u}_{\mathrm{U},j}\|^2. \tag{28}$$

Then, at a feasible point $(\eta_{\mathrm{U},j,j'}^{(n)}, \beta_{\mathrm{U},j}^{(n)}, t_{\mathrm{DU},j}^{(n)})$, it can be shown in a manner similar to (22) that

$$\ln(1+\bar{r}_{\mathrm{U},j}) \geqslant Z(\bar{\gamma}_{\mathrm{U},j}, \beta_{\mathrm{U},j}, \bar{\gamma}_{\mathrm{U},j}^{(n)}, \beta_{\mathrm{U},j}^{(n)}). \tag{29}$$

By now, we have approximated the nonconvex item $\sum_{k\in\mathcal{K}} R_{\mathrm{D},k} + \sum_{j\in\mathcal{J}} R_{\mathrm{U},j}$ in the objective function by the convex lower bound

$$F(R_{\mathrm{D},k}, R_{\mathrm{U},j}) = \sum_{k\in\mathcal{K}} Z(\gamma_{\mathrm{D},k}, \lambda_{\mathrm{D},k}, \gamma_{\mathrm{D},k}^{(n)}, \lambda_{\mathrm{D},k}^{(n)}) + \sum_{j\in\mathcal{J}} Z(\bar{\gamma}_{\mathrm{U},j}, \beta_{\mathrm{U},j}, \bar{\gamma}_{\mathrm{U},j}^{(n)}, \beta_{\mathrm{U},j}^{(n)}). \tag{30}$$

Next, in a similar manner to (17c), the constraint (11f) can be approximated by

$$\hat{Z}(\boldsymbol{Q}_{\mathrm{D}}^{(0)}\boldsymbol{w}_{\mathrm{D},k}, \boldsymbol{Q}_{\mathrm{D}}^{(0)}\boldsymbol{w}_{\mathrm{D},k}^{(n)}, \boldsymbol{G}_{\mathrm{D},k}) \geqslant r_{\mathrm{D},\min,k}\left(\sum_{k'\neq k,k\in\mathcal{K}}|\boldsymbol{g}_{\mathrm{D},k}^{\mathrm{H}}\boldsymbol{Q}_{\mathrm{D}}^{(0)}\boldsymbol{w}_{\mathrm{D},k'}|^2+\sum_{j\in\mathcal{J}}P_{\mathrm{U},j}|h_{\mathrm{IUI},j,k}|^2+\sigma_{\mathrm{D},k}^2\right). \quad (31)$$

To derive (31), we have used the fact that constraint (11f) can be rewrote as

$$|\boldsymbol{g}_{\mathrm{D},k}^{\mathrm{H}}\boldsymbol{Q}_{\mathrm{D}}^{(0)}\boldsymbol{w}_{\mathrm{D},k}|^2 \geqslant r_{\mathrm{D},\min,k}\left(\sum_{k'\neq k,k\in\mathcal{K}}|\boldsymbol{g}_{\mathrm{D},k}^{\mathrm{H}}\boldsymbol{Q}_{\mathrm{D}}^{(0)}\boldsymbol{w}_{\mathrm{D},k'}|^2+\sum_{j\in\mathcal{J}}P_{\mathrm{U},j}|h_{\mathrm{IUI},j,k}|^2+\sigma_{\mathrm{D},k}^2\right).$$

Then, we can obtain the constraint (31) according to (17c).

Finally, according to the above approximation, i.e., the inequations (23a) and (25a)–(25c), the constraint (11g) can be approximated by the following SOC convex constraint:

$$\|\boldsymbol{z}_{\mathrm{U},j}\|_2 \leqslant \beta_{\mathrm{U},j}, \quad (32)$$

where

$$\begin{aligned}\boldsymbol{z}_{\mathrm{U},j} = {}& \sqrt{r_{\mathrm{U},\min,j}}\,[\delta_{\mathrm{IRI}}t_{\mathrm{DU},1},\ldots,\delta_{\mathrm{IRI}}t_{\mathrm{DU},j},\ldots,\delta_{\mathrm{IRI}}t_{\mathrm{DU},J},\eta_{\mathrm{U},j,1},\ldots,\eta_{\mathrm{U},j,j-1},\eta_{\mathrm{U},j,j+1},\ldots,\eta_{\mathrm{U},j,J},\\ & \sigma_{\mathrm{U},1}\mathrm{vec}(\tilde{\boldsymbol{u}}_{\mathrm{U},j,1}),\ldots,\sigma_{\mathrm{U},X}\mathrm{vec}\,(\tilde{\boldsymbol{u}}_{\mathrm{U},j,X})]\,,\\ \tilde{\boldsymbol{u}}_{\mathrm{U},j,x'} = {}& \boldsymbol{Q}_{\mathrm{U},x'}^{(0)}\boldsymbol{u}_{\mathrm{U},j,x'}.\end{aligned}$$

To summarize, given $\boldsymbol{q}_{\mathrm{D},x}^{(n)}$ and $\boldsymbol{q}_{\mathrm{U},x'}^{(n)}$, the nonconvex object and the constraints (11f) and (11g) can be approximated by the convex constraints (20), (22), (27), (29), (31), (32), (23a), and (25a)–(25c). As a result, problem (16) can be approximated by the following convex problem:

$$\begin{aligned}&\max_{\{\boldsymbol{w}_{\mathrm{D},k},\boldsymbol{u}_{\mathrm{U},j},P_{\mathrm{U},j}\}} \quad F\left(R_{\mathrm{D},k},R_{\mathrm{U},j}\right)\\ &\text{s.t. (11b), (11c), (20), (22), (27), (29), (31), (32), (23a), (25a), (25b), (25c).}\end{aligned} \quad (33)$$

Since problem (33) is a convex problem, it can be globally solved by CVX [32] or interior-point methods [33]. The SCA method-based algorithm to solve problem (16) with fixed $\boldsymbol{q}_{\mathrm{D},x}^{(n)}$ and $\boldsymbol{q}_{\mathrm{U},x'}^{(n)}$ is summarized in Algorithm 2.

Algorithm 2 Solution to problem (16) with SCA-based algorithm

Input: Initialization: $\boldsymbol{Q}_{\mathrm{D}}^{(0)}$, $\boldsymbol{Q}_{\mathrm{U}}^{(0)}$, $\boldsymbol{w}_{\mathrm{D},k}^{(0)}$, $\boldsymbol{u}_{\mathrm{U},j}^{(0)}$, $P_{\mathrm{U},j}^{(0)}$.
1: **repeat**
2: Solve (33) with fixed duplex mode $\boldsymbol{Q}_{\mathrm{D}}^{(n)}\to\boldsymbol{Q}_{\mathrm{D}}^{(0)}$, $\boldsymbol{Q}_{\mathrm{U}}^{(n)}\to\boldsymbol{Q}_{\mathrm{U}}^{(0)}$, and denote the optimal solutions as $(\boldsymbol{w}_{\mathrm{D},k}^{\dagger},\boldsymbol{u}_{\mathrm{U},j}^{\dagger},P_{\mathrm{U},j}^{\dagger})$;
3: Update $\boldsymbol{w}_{\mathrm{D},k}^{(n)}\to\boldsymbol{w}_{\mathrm{D},k}^{\dagger}$, $\boldsymbol{u}_{\mathrm{U},j}^{(n)}\to\boldsymbol{u}_{\mathrm{U},j}^{\dagger}$, $P_{\mathrm{U},j}^{(n)}\to P_{\mathrm{U},j}^{\dagger}$;
4: Set $n\to n+1$;
5: **until** convergence;
6: **return** the optimal solutions $(\boldsymbol{w}_{\mathrm{D},k}^{\dagger},\boldsymbol{u}_{\mathrm{U},j}^{\dagger},P_{\mathrm{U},j}^{\dagger})$.

4.2 Stage II: solution for problem (12) with fixed transceivers

When the transceivers are fixed, the problem (12) becomes

$$\begin{aligned}&\max_{\{\boldsymbol{q}_{\mathrm{D}},\boldsymbol{q}_{\mathrm{U}}\}} \quad \sum_{k\in\mathcal{K}}R_{\mathrm{D},k}+\sum_{j\in\mathcal{J}}R_{\mathrm{U},j}-f\left(q_{\mathrm{D},x,m},q_{\mathrm{U},x',m'}\right)\\ &\text{s.t. (11b), (11c), (11f), (11g), (12b), (12c), (12d),}\end{aligned} \quad (34)$$

with $\boldsymbol{w}_{\mathrm{D},k}=\boldsymbol{w}_{\mathrm{D},k}^{(0)}$, $\boldsymbol{u}_{\mathrm{U},j}=\boldsymbol{u}_{\mathrm{U},j}^{(0)}$, and $P_{\mathrm{U},j}=P_{\mathrm{U},j}^{(0)}$.

Similar to (22), $R_{\mathrm{D},k}$ can be lower-bounded by

$$\ln(1+r_{\mathrm{D},k}) \geqslant Z(\gamma_{\mathrm{D},k},\bar{\lambda}_{\mathrm{D},k},\gamma_{\mathrm{D},k}^{(n)},\bar{\lambda}_{\mathrm{D},k}^{(n)}) \quad (35)$$

with the linear constraint as

$$\bar{\lambda}_{\mathrm{D},k} \geqslant 0, \tag{36}$$

and convex constraint as

$$\hat{Z}(\boldsymbol{Q}_{\mathrm{D}}\boldsymbol{w}_{\mathrm{D},k}^{(0)}, \boldsymbol{Q}_{\mathrm{D}}^{(n)}\boldsymbol{w}_{\mathrm{D},k}^{(0)}, \boldsymbol{G}_{\mathrm{D},k}) \geqslant \bar{\lambda}_{\mathrm{D},k}^2, \tag{37}$$

where $\bar{\lambda}_{\mathrm{D},k}$ is a newly introduced variable.

Next, similar to (23a), by introducing a series of variables $\{\bar{\alpha}_{\mathrm{D}}\}$, $\{\bar{t}_{\mathrm{DU},j}\}$, Eq. (9) can be approximated by

$$P_{\mathrm{U},j}^{(0)}|(\boldsymbol{u}_{\mathrm{U},j}^{(0)})^{\mathrm{H}}\boldsymbol{Q}_{\mathrm{U}}\boldsymbol{g}_{\mathrm{U},j}|^2 \geqslant \bar{\beta}_{\mathrm{U},j}^2, \tag{38a}$$

$$\sum_{k\in\mathcal{K}} \|\boldsymbol{Q}_{\mathrm{D}}\boldsymbol{w}_{\mathrm{D},k}^{(0)}\|^2 \leqslant \bar{\alpha}_{\mathrm{D}}, \tag{38b}$$

$$\bar{\alpha}_{\mathrm{D}}\|\boldsymbol{Q}_{\mathrm{U}}\boldsymbol{u}_{\mathrm{U},j}^{(0)}\|^2 \leqslant \bar{t}_{\mathrm{DU},j}^2. \tag{38c}$$

Further, (38a) and (38c) can be approximated as

$$P_{\mathrm{U},j}^{(0)}\hat{Z}\big((\boldsymbol{u}_{\mathrm{U},j}^{(0)})^{\mathrm{H}}\boldsymbol{Q}_{\mathrm{U}}, (\boldsymbol{u}_{\mathrm{U},j}^{(0)})^{\mathrm{H}}\boldsymbol{Q}_{\mathrm{U}}^{(n)}, \boldsymbol{G}_{\mathrm{U},j}\big) \geqslant \bar{\beta}_{\mathrm{U},j}^2, \tag{39a}$$

$$\|\boldsymbol{Q}_{\mathrm{U}}\boldsymbol{u}_{\mathrm{U},j}^{(0)}\|^2 \leqslant \bar{Z}(\bar{\alpha}_{\mathrm{D}}, \bar{t}_{\mathrm{DU},j}, \bar{\alpha}_{\mathrm{D}}^{(n)}, \bar{t}_{\mathrm{DU},j}^{(n)}), \tag{39b}$$

where $\boldsymbol{G}_{\mathrm{U},j} = \boldsymbol{g}_{\mathrm{U},j}\boldsymbol{g}_{\mathrm{U},j}^{\mathrm{H}}$.

Then, the lower bound of (9) can be expressed as

$$\tilde{r}_{\mathrm{U},j} \geqslant \frac{\bar{\beta}_{\mathrm{U},j}^2}{\tilde{\gamma}_{\mathrm{U},j}} \tag{40}$$

with the linear constraint as

$$\bar{\beta}_{\mathrm{U},j} \geqslant 0, \tag{41}$$

and where

$$\tilde{\gamma}_{\mathrm{U},j} = P_{\mathrm{U},j'}^{(0)}|(\boldsymbol{u}_{\mathrm{U},j}^{(0)})^{\mathrm{H}}\boldsymbol{Q}_{\mathrm{U}}\boldsymbol{g}_{\mathrm{U},j'}|^2 + \delta_{\mathrm{IRI}}^2\bar{t}_{\mathrm{DU},j}^2 + \sum_{x'\in\mathcal{X}} \sigma_{\mathrm{U},x'}^2\|\boldsymbol{Q}_{\mathrm{U}}\boldsymbol{u}_{\mathrm{U},j}^{(0)}\|^2, \tag{42}$$

and $\tilde{\gamma}_{\mathrm{U},j}$ is a newly introduced variable.

Additionally, similar to (29), the lower bound of $R_{\mathrm{U},j}$ is

$$\ln(1+\tilde{r}_{\mathrm{U},j}) \geqslant Z(\tilde{\gamma}_{\mathrm{U},j}, \bar{\beta}_{\mathrm{U},j}, \tilde{\gamma}_{\mathrm{U},j}^{(n)}, \bar{\beta}_{\mathrm{U},j}^{(n)}). \tag{43}$$

Further, we can approximate the nonconvex item $\sum_{k\in\mathcal{K}} R_{\mathrm{D},k} + \sum_{j\in\mathcal{J}} R_{\mathrm{U},j}$ in the objective function by the convex lower bound

$$\bar{F}(R_{\mathrm{D},k}, R_{\mathrm{U},j}) = \sum_{k\in\mathcal{K}} Z(\gamma_{\mathrm{D},k}, \bar{\lambda}_{\mathrm{D},k}, \gamma_{\mathrm{D},k}^{(n)}, \bar{\lambda}_{\mathrm{D},k}^{(n)}) + \sum_{j\in\mathcal{J}} Z(\tilde{\gamma}_{\mathrm{U},j}, \bar{\beta}_{\mathrm{U},j}, \tilde{\gamma}_{\mathrm{U},j}^{(n)}, \bar{\beta}_{\mathrm{U},j}^{(n)}). \tag{44}$$

Moreover, we observe that given ε, the function $f(q_{\mathrm{D},x,m}, q_{\mathrm{U},x',m'})$ in the objective function is concave, and the objective can be considered as a difference of the concave function. Therefore, we linearize the logarithmic penalty function by its first-order Taylor approximation as

$$\begin{aligned}
&\tilde{f}(q_{\mathrm{D},x,m}, q_{\mathrm{U},x',m'}, q_{\mathrm{D},x,m}^{(n)}, q_{\mathrm{U},x',m'}^{(n)}) \\
&= f(q_{\mathrm{D},x,m}^{(n)}, q_{\mathrm{U},x',m'}^{(n)}) + \sum_{x\in\mathcal{X}}\sum_{m\in\mathcal{X}_m}\left(\frac{1}{q_{\mathrm{D},x,m}^{(n)}+\varepsilon} - \frac{1}{(1-q_{\mathrm{D},x,m}^{(n)})+\varepsilon}\right)(q_{\mathrm{D},x,m} - q_{\mathrm{D},x,m}^{(n)}) \\
&\quad + \sum_{x'\in\mathcal{X}}\sum_{m'\in\mathcal{X}_{m'}}\left(\frac{1}{q_{\mathrm{U},x',m'}^{(n)}+\varepsilon} - \frac{1}{(1-q_{\mathrm{U},x',m'}^{(n)})+\varepsilon}\right)(q_{\mathrm{U},x',m'} - q_{\mathrm{U},x',m'}^{(n)}).
\end{aligned} \tag{45}$$

Since the function $f(q_{\mathrm{D},x,m}, q_{\mathrm{U},x',m'})$ is concave, the first-order Taylor approximation function (45) should be served as its upper bound. Furthermore, $\bar{F}(R_{\mathrm{D},k}, R_{\mathrm{U},j})$ is the lower bound of function $\sum_{k\in\mathcal{K}} R_{\mathrm{D},k} + \sum_{j\in\mathcal{J}} R_{\mathrm{U},j}$. To summarize, the lower bound of the objective function is

$$\sum_{k\in\mathcal{K}} R_{\mathrm{D},k} + \sum_{j\in\mathcal{J}} R_{\mathrm{U},j} - f(q_{\mathrm{D},x,m}, q_{\mathrm{U},x',m'}) \geqslant \bar{F}(R_{\mathrm{D},k}, R_{\mathrm{U},j}) - \tilde{f}(q_{\mathrm{D},x,m}, q_{\mathrm{U},x',m'}, q^{(n)}_{\mathrm{D},x,m}, q^{(n)}_{\mathrm{U},x',m'}). \tag{46}$$

In the following, we address the QoS constraints (11f) and (11g) in (34). By following a similar methodology as (31) and (32), the two constraints can be approximated by

$$\hat{Z}(\boldsymbol{Q}_{\mathrm{D}}\boldsymbol{w}^{(0)}_{\mathrm{D},k}, \boldsymbol{Q}^{(n)}_{\mathrm{D}}\boldsymbol{w}^{(0)}_{\mathrm{D},k}, \boldsymbol{g}_{\mathrm{D},k}) \geqslant r_{\mathrm{D},\min,k}\left(\sum_{k'\neq k,k\in\mathcal{K}} |\boldsymbol{g}^{\mathrm{H}}_{\mathrm{D},k}\boldsymbol{Q}_{\mathrm{D}}\boldsymbol{w}^{(0)}_{\mathrm{D},k'}|^2 + \sum_{j\in\mathcal{J}} P^{(0)}_{\mathrm{U},j}|h_{\mathrm{IUI},j,k}|^2 + \sigma^2_{\mathrm{D},k}\right), \tag{47a}$$

$$\sum_{k\in\mathcal{K}} \|\boldsymbol{Q}_{\mathrm{D}}\boldsymbol{w}^{(0)}_{\mathrm{D},k}\|^2 \leqslant \bar{\alpha}_{\mathrm{D}}, \tag{47b}$$

$$\|\boldsymbol{Q}_{\mathrm{U}}\boldsymbol{u}^{(0)}_{\mathrm{U},j}\|^2 \leqslant \bar{Z}(\bar{\alpha}_{\mathrm{D}}, \bar{t}_{\mathrm{DU},j}, \bar{\alpha}^{(n)}_{\mathrm{D}}, \bar{t}^{(n)}_{\mathrm{DU},j}), \tag{47c}$$

$$\|\tilde{\boldsymbol{z}}_{\mathrm{U},j}\|_2 \leqslant \bar{\beta}_{\mathrm{U},j}, \tag{47d}$$

where

$$\begin{aligned}\bar{\boldsymbol{z}}_{\mathrm{U},j} = \sqrt{r_{\mathrm{U},\min,j}}\Big[&\delta_{\mathrm{IRI}}\bar{t}_{\mathrm{DU},1}, \ldots, \delta_{\mathrm{IRI}}\bar{t}_{\mathrm{DU},j}, \ldots, \delta_{\mathrm{IRI}}\bar{t}_{\mathrm{DU},J}\sqrt{P^{(0)}_{\mathrm{U},1}}\Re\big((\boldsymbol{u}^{(0)}_{\mathrm{U},j})^{\mathrm{H}}\boldsymbol{Q}_{\mathrm{U}}\boldsymbol{g}_{\mathrm{U},1}\big), \ldots,\\ &\sqrt{P^{(0)}_{\mathrm{U},j-1}}\Re\big((\boldsymbol{u}^{(0)}_{\mathrm{U},j})^{\mathrm{H}}\boldsymbol{Q}_{\mathrm{U}}\boldsymbol{g}_{\mathrm{U},j-1}\big), \sqrt{P^{(0)}_{\mathrm{U},j+1}}\Re\big((\boldsymbol{u}^{(0)}_{\mathrm{U},j})^{\mathrm{H}}\boldsymbol{Q}_{\mathrm{U}}\boldsymbol{g}_{\mathrm{U},j+1}\big), \ldots,\\ &\sqrt{P^{(0)}_{\mathrm{U},J}}\Re\big((\boldsymbol{u}^{(0)}_{\mathrm{U},j})^{\mathrm{H}}\boldsymbol{Q}_{\mathrm{U}}\boldsymbol{g}_{\mathrm{U},J}\big), \mathrm{vec}(\tilde{\boldsymbol{u}}_{\mathrm{U},j,1})\sigma_{\mathrm{U},1}, \ldots, \mathrm{vec}(\tilde{\boldsymbol{u}}_{\mathrm{U},j,X})\sigma_{\mathrm{U},X}\Big],\end{aligned} \tag{48}$$

and

$$\tilde{\boldsymbol{u}}_{\mathrm{U},j,x'} = \boldsymbol{Q}^{(0)}_{\mathrm{U},x'}\boldsymbol{u}_{\mathrm{U},j,x'}. \tag{49}$$

Then, given $P^{(n)}_{\mathrm{U},j}$, $\boldsymbol{u}^{(n)}_{\mathrm{U},j}$, and $\boldsymbol{w}^{(n)}_{\mathrm{D},k}$, the nonconvex objective and the constraints (11f) and (11g) can be approximated by the convex constraints (46) and (47a)–(47d). As a result, problem (14) can be approximated by the following convex problem:

$$\begin{aligned}\max_{\{\boldsymbol{q}_{\mathrm{D}},\boldsymbol{q}_{\mathrm{U}}\}}\ & \bar{F}(R_{\mathrm{D},k}, R_{\mathrm{U},j}) - \tilde{f}(q_{\mathrm{D},x,m}, q_{\mathrm{U},x',m'}, q^{(n)}_{\mathrm{D},x,m}, q^{(n)}_{\mathrm{U},x',m'})\\ \text{s.t.}\ & (12\text{b}),\ (12\text{c}),\ (12\text{d}),\ (11\text{b}),\ (11\text{c}),\ (36),\ (37),\ (41),\\ & (39\text{a}),\ (39\text{b}),\ (47\text{a}),\ (47\text{b}),\ (47\text{c}),\ (47\text{d}).\end{aligned} \tag{50}$$

The SCA method-based algorithm to solve problem (34) with fixed $\{\boldsymbol{w}_{\mathrm{D},k}, \boldsymbol{u}_{\mathrm{U},j}, P_{\mathrm{U},j}\}$ is summarized in Algorithm 3.

Algorithm 3 Solution to problem (34) with SCA-based algorithm

Input: Initialization: $\boldsymbol{Q}^{(0)}_{\mathrm{D}}$, $\boldsymbol{Q}^{(0)}_{\mathrm{U}}$, $\boldsymbol{w}^{(0)}_{\mathrm{D},k}$, $\boldsymbol{u}^{(0)}_{\mathrm{U},j}$, $P^{(0)}_{\mathrm{U},j}$.
1: **repeat**
2: Solve (50) with fixed transmitters $\boldsymbol{w}^{(n)}_{\mathrm{D},k} \to \boldsymbol{w}^{(0)}_{\mathrm{D},k}$, $\boldsymbol{u}^{(n)}_{\mathrm{U},j} \to \boldsymbol{u}^{(0)}_{\mathrm{U},j}$, $P^{(n)}_{\mathrm{U},j} \to P^{(0)}_{\mathrm{U},j}$, and denote the optimal solutions as $(\boldsymbol{Q}^{\dagger}_{\mathrm{D}}, \boldsymbol{Q}^{\dagger}_{\mathrm{U}})$;
3: Update $\boldsymbol{Q}^{(n+1)}_{\mathrm{D}} \to \boldsymbol{Q}^{\dagger}_{\mathrm{D}}$, $\boldsymbol{Q}^{(n+1)}_{\mathrm{U}} \to \boldsymbol{Q}^{\dagger}_{\mathrm{U}}$;
4: Set $n \to n+1$;
5: **until** convergence;
6: **return** the optimal solutions $(\boldsymbol{Q}^{\dagger}_{\mathrm{D}}, \boldsymbol{Q}^{\dagger}_{\mathrm{U}})$.

4.3 Overall complexity to solve problem (12)

Since the subproblems (33) and (50) only contains quadratic constraints and linear constraints, and the the quadratic constraints can be further transformed into SOC constraints, the proposed algorithm of solving problem (12) has a low complexity. In particular, subproblem (33) has $KXM + J + k + J^2$ scalar variables and $7J + 3K + X + 1$ constraints, subproblem (50) has $2XM + 3J + K + 1$ scalar variables

Table 1 Simulation parameters

Parameter	Value
Radius	60 m
Power constraint for RAU/User	1 W/0.1 W
Number of downlink users/uplink users	4/4
Path loss	$128.1 + 37.6\log10(d)$
Lognormal shadowing/Rayleigh fading	8 dB/0 dB
Noise power ($\sigma^2_{\mathrm{U},z} = \sigma^2_{\mathrm{D},k} = \sigma^2$)	-70 dBm

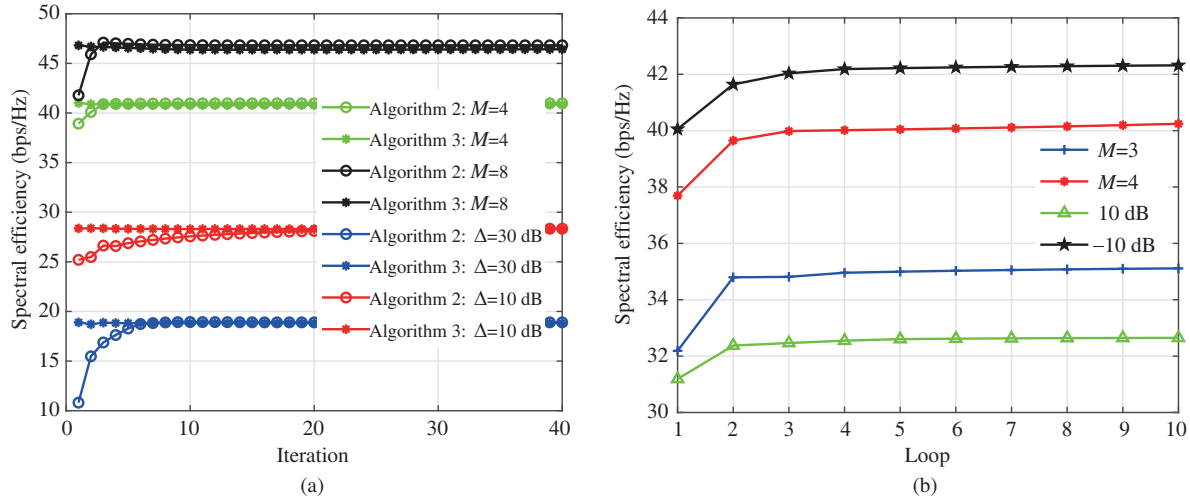

Figure 2 (Color online) The convergence behavior of SE performance versus iteration/loop for $\Delta = -10/10/30$ dB, $M = 3/4/8$. (a) The convergence behavior of SE versus iteration; (b) the convergence behavior of SE versus loop.

and $6XM + X + 5J + 2K + 1$ constraints. Hence, the proposed Algorithm 1 takes a polynomial time complexity $O(V_{\mathrm{com}})$, where $V_{\mathrm{com}} = (7J + 3K + X + 1)^{2.5}(KXM + J + k + J^2)^2 + (7J + 3K + X + 1)^{3.5} + (6XM + X + 5J + 2K + 1)^{2.5}(2XM + 3J + K + 1)^2 + (6XM + X + 5J + 2K + 1)^{3.5}$ [34, 35]. Supposing the two subproblems run at most T_{tot} loops, then the overall complexity of solving problem (12) is at most $O(V_{\mathrm{com}}T_{\mathrm{tot}})$. With the same spirit, the complexity of EXH, exhaustive search solution is $O(3^{MX}((7J + 3K + X + 1)^{2.5}(KXM + J + k + J^2)^2 + (7J + 3K + X + 1)^{3.5}))$. Due to the fact that the number of RAUs in cell-free massive MIMO is very large, the complexity of EXH is obvious far higher than the proposed algorithm.

5 Numerical results

In this section, some numerical examples are evaluated to show the performance of the proposed algorithms under different system settings. We consider a cell-free massive MIMO system in a circular area with the detailed simulation parameters listed in Table 1. For simplicity, we model the residual interference power between T-RAU x and R-RAU x' as $\delta_{\mathrm{IRI},x,x'} = \Delta_{\mathrm{IRI},x,x'}\sigma^2 = \Delta\sigma^2$, where $\Delta_{\mathrm{IRI},x,x'} = \Delta, \forall x, x'$ represents the ratio of the channel estimation error.

Figure 2 shows the convergence behavior of Algorithms 1–3 for problem (12). It can be observed that the proposed Algorithms 1–3 converge roughly within 2–4 loops, 5–12 iterations, and 1–2 iterations, respectively.

Then, SE versus channel estimation error is given in Figure 3. A general observation is that the proposed algorithm maintains a high average sum SE and is close to the optimal EXH for different IRI cancellation capabilities. Moreover, the spectral efficiencies of the two schemes are close to each other when $\Delta \geqslant -5$ dB, and the gap slightly increases when $\Delta > -5$ dB. This behavior is explained by the possibility of a better chance to find the mode condition to overcome the impact of IRI in EXH when Δ is large. Furthermore, as expected, when $\Delta \leqslant 15$ dB, the proposed algorithm achieves the highest SE, followed by greedy algorithm (Greedy), cloud radio access network (C-RAN) CCFD and TDD scheme, and random algorithm (Random) obtain the lowest SE. Specifically, as shown in Figure 3, the gap between

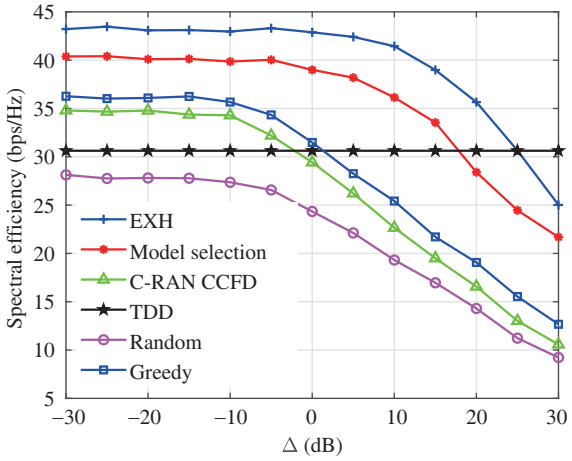

Figure 3 (Color online) The SE versus IRI for $R_{\mathrm{D},\min,k} = R_{\mathrm{U},\min,j} = 0.1$ bps/Hz, $M = 2$.

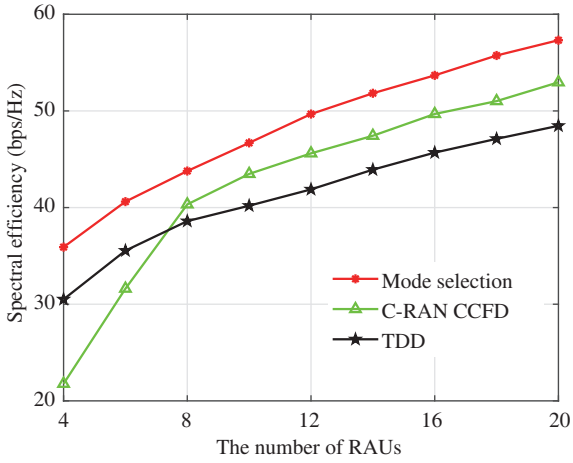

Figure 4 (Color online) The SE versus the number of RAUs for $R_{\mathrm{D},\min,k} = R_{\mathrm{U},\min,j} = 1$ bps/Hz, $\Delta = 10$ dB.

the proposed algorithm and C-RAN CCFD is obvious when $\Delta \geqslant -5$ dB, for example, when Δ reduces to 15 and -20 dB, the total SE gap of the two schemes is 14.04 and 5.31 bps/Hz, respectively. Also, as we can see, C-RAN CCFD has a close SE performance to Greedy, and the average gap between the two schemes is about 4.6 bps/Hz. It is interesting that the SE of Random is close to C-RAN CCFD when $\Delta \geqslant 10$ dB, and the gap of the two schemes becomes higher when $\Delta \leqslant 15$ dB. As a result, we can conclude that the proposed algorithm can achieve better performance gains than the C-RAN CCFD, greedy algorithm and random algorithm, especially when the IRI is not suppressed well. Notice that although the SE of the proposed algorithm and the EXH is lower than the TDD scheme when Δ is high. However, the proposed scheme and the other duplex mode schemes consider both uplink and downlink QoS constraints simultaneously. This is practical because low latency is one of the major parameters for 5G or beyond 5G wireless cellular systems. Hence, the TDD strategy is not considered in the proposed algorithm and the other duplex mode schemes.

Next, Figure 4 shows the SE versus the number of RAUs, where $\Delta = 10$ dB. We observe that the SE of all algorithms rapidly increases with the increase in the number of RAUs. Specifically, when the total number of RAUs is less than 6, the proposed algorithm achieves the best SE performance, while the TDD scheme achieves better SE performance than the C-RAN CCFD scheme. When the total number of RAUs is larger than 6, the best SE performance is also achieved by the proposed algorithm, followed by the C-RAN CCFD scheme, and the worst SE performance achieved by the TDD scheme. Furthermore, the gap between the proposed algorithm and the TDD scheme decreases when increasing the number of RAUs. For example, the gap increases from approximately 5.40 bps/Hz when using 4 RAUs, to approximately 8.55 bps/Hz when using 20 RAUs. The reason is that when the IRI is 10 dB and the total number of RAU is less than 6, the system does not have enough freedom to overcome the negative impact of high IRI. On the contrary, the deployment of a large number of RAU can provide users with a closer access distance, which further helps to provide more dimensions to design appropriate transceivers to overcome IRI. Hence, we can conclude that the increased number of RAUs can help to suppress the IRI in CCFD and NAFD schemes.

Figure 5 demonstrates the SE performance comparison between the proposed mode selection, C-RAN CCFD and TDD scheme versus the number of antennas for each RAU. From the plot, we can observe that the proposed mode selection algorithm outperforms the C-RAN CCFD and TDD counterparts. When $M \leqslant 5$, the best performance is achieved by the proposed mode selection algorithm, followed by the TDD scheme, and the C-RAN CCFD scheme yields the worst SE performance. However, when $M \geqslant 5$, the SE performance order of the three schemes is the proposed mode selection algorithm, the C-RAN CCFD scheme and the TDD scheme. Hence, we can find that the proposed mode selection scheme has a better performance than the TDD scheme and the C-RAN CCFD scheme. In addition, it can be observed that the increased number of antennas for each RAU can produce a great benefit for the C-RAN CCFD scheme to reduce the negative impact of IRI, especially when IRI is serious. Furthermore, we also notice that the gap between the proposed mode selection scheme and the C-RAN CCFD scheme decreases with

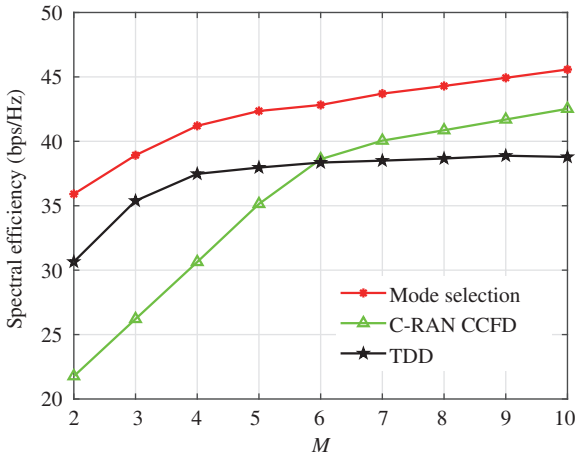

Figure 5 (Color online) The SE versus the number of antennas for each RAU with $R_{\mathrm{D},\min,k} = R_{\mathrm{U},\min,j} = 1$ bps/Hz, $\Delta = 10$ dB.

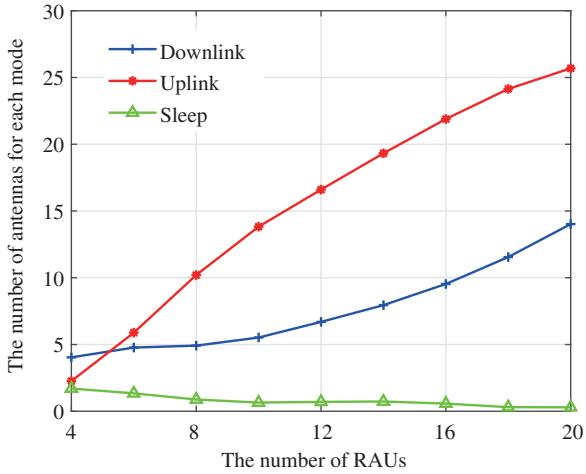

Figure 6 (Color online) The number of antennas for each mode versus the number of RAUs.

the increase in the number of antennas, while the gap between the proposed mode selection scheme and the TDD scheme increases. For example, the gap between the proposed mode selection scheme and the C-RAN CCFD scheme decreases from approximately 16 bps/Hz when using 2 antennas to approximately 3.05 bps/Hz when using 10 antennas, while the gap between the latter two schemes is 5.3 and 6.79 bps/Hz, respectively. Intuitively, this is true because when the number of antennas increased, the IRI reaches saturation or increases a little due to the power constraint for downlink beamforming. Hence, the effect of IRI becomes less when the number of antennas increases. This behavior implies that when compared with the C-RAN CCFD scheme, the role of mode selection is small when the number of antennas is large, and conversely when compared with the TDD scheme.

In Figure 6, we illustrate the number of antennas for each mode versus the number of RAUs. As we can see, the number of transmitting antennas and receiving antennas increased with the growing number of antennas, and the number of sleep antennas decreased. Specifically, the number of receiving antennas increased faster than transmitting antennas; for example, when $X = 4$, the number of transmitting antennas and receiving antennas is 4 and 2.3, respectively, and the number of antennas increased to 14 and 25.7 when $X = 20$. Intuitively, this is true because when the number of RAUs increases, the IRI becomes serious. To mitigate IRI and improve the SE, the system needs more antennas to operate in uplink mode and downlink mode. Furthermore, the transmission power transmitted by uplink users is much less than that of RAUs. Hence, more antennas to detect the uplink signal is an effective method to improve the uplink SE and the total SE. As a result, in order to maximize the total SE, the system needs a massive number of receiving antennas to detect the uplink signals and slightly increases the number of transmitting antennas to reduce the IRI. At the same time, when the number of total antennas increases, the system needs fewer sleep antennas. This is benefit by the joint optimize of the transceivers. In addition, we can conclude that the more degree of freedom for RAUs, the fewer sleep antennas will be.

6 Conclusion

In this paper, we consider the fundamental problem of duplex mode selection for a cell-free massive MIMO with NAFD. Specifically, our objective was to maximize the SE of downlink and uplink users, where the QoS constraints and power budget constraints are considered. To handle the highly coupled problem, we have proposed a two-stage duplex mode selection and transceiver design algorithm. Specifically, in the first stage, we set each element of the mode selection vectors as 0.5 and optimize the transceivers. In the second stage, with the transceivers obtained from the first stage, we further optimize the duplex mode selection. Simulation results have demonstrated that the proposed solution can obtain a close performance to the optimal EXH and a better performance than the C-RAN CCFD scheme. We also have shown that, compared with the C-RAN CCFD scheme, the more serious the IRI, the higher the SE

gains that will be obtained by the proposed mode selection algorithm.

Acknowledgements This work was supported in part by National Key Research and Development Program (Grant No. 2018YFE0205902), National Natural Science Foundation of China (NSFC) (Grant Nos. 61871122, 61971127, 61871465, 61801168).

References

1 Wang J Y, Dai L. Downlink rate analysis for virtual-cell based large-scale distributed antenna systems. IEEE Trans Wirel Commun, 2015, 15: 1998–2011
2 Li J M, Wang D M, Zhu P C, et al. Impacts of practical channel impairments on the downlink spectral efficiency of large-scale distributed antenna systems. Sci China Inf Sci, 2019, 62: 022303
3 Shojaeifard A, Wong K K, Yu W, et al. Full-duplex cloud radio access network: stochastic design and analysis. IEEE Trans Wirel Commun, 2018, 17: 7190–7207
4 Nguyen D, Tran L N, Pirinen P, et al. On the spectral efficiency of full-duplex small cell wireless systems. IEEE Trans Wirel Commun, 2014, 13: 4896–4910
5 Yadav A, Dobre O A, Poor H V. Is self-interference in full-duplex communications a foe or a friend? IEEE Signal Process Lett, 2018, 25: 951–955
6 Riihonen T, Werner S, Wichman R. Mitigation of loopback self-interference in full-duplex MIMO relays. IEEE Trans Signal Process, 2011, 59: 5983–5993
7 Koh J, Lim Y G, Chae C B, et al. On the feasibility of full-duplex large-scale MIMO cellular systems. IEEE Trans Wirel Commun, 2018, 17: 6231–6250
8 Bharadia D, McMilin E, Katti S. Full duplex radios. In: Proceedings of ACM SIGCOMM Computer Communication Review, 2013. 375–386
9 Thomsen H, Popovski P, de Carvalho E, et al. CoMPflex: CoMP for in-band wireless full duplex. IEEE Wirel Commun Lett, 2015, 5: 144–147
10 Xin Y X, Zhang R Q, Wang D M, et al. Antenna clustering for bidirectional dynamic network with large-scale distributed antenna systems. IEEE Access, 2017, 5: 4037–4047
11 Xin Y X, Yang L Q, Wang D M, et al. Bidirectional dynamic networks with massive MIMO: performance analysis. IET Commun, 2017, 11: 468–476
12 Wang D M, Zhao Z L, Huang Y Q, et al. Large-scale multi-user distributed antenna system for 5G wireless communications. In: Proceedings of the 81st Vehicular Technology Conference (VTC Spring), 2015. 1–5
13 Vu T T, Ngo D T, Ngo H Q, et al. Full-duplex cell-free massive MIMO. In: Proceedings of IEEE International Conference on Communications (ICC), 2019. 1–6
14 Nguyen V H, Nguyen V D, Dobre O A, et al. A novel heap-based pilot assignment for full duplex cell-free massive MIMO with zero-forcing. In: Proceedings of IEEE International Conference on Communications (ICC), 2020. 1–6
15 Nguyen H V, Nguyen V D, Dobre O A, et al. Joint antenna array mode selection and user assignment for full-duplex MU-MISO systems. IEEE Trans Wirel Commun, 2019, 18: 2946–2963
16 Wang D M, Wang M H, Zhu P C, et al. Performance of network-assisted full-duplex for cell-free massive MIMO. IEEE Trans Commun, 2020, 68: 1464–1478
17 Xia X J, Zhu P C, Li J M, et al. Joint sparse beamforming and power control for a large-scale DAS with network-assisted full duplex. IEEE Trans Veh Technol, 2020, 69: 7569–7582
18 Wu F, Xu Q, Shao S H, et al. Performance of auxiliary antenna-based self-interference cancellation in full-duplex radios. Sci China Inf Sci, 2018, 61: 109307
19 Simeone O, Erkip E, Shamai S. Full-duplex cloud radio access networks: an information-theoretic viewpoint. IEEE Wirel Commun Lett, 2014, 3: 413–416
20 Mohammadi M, Suraweera H A, Tellambura C. Uplink/downlink rate analysis and impact of power allocation for full-duplex cloud-RANs. IEEE Trans Wirel Commun, 2018, 17: 5774–5788
21 Zhao M M, Shi Q J, Cai Y L, et al. Joint transceiver design for full-duplex cloud radio access networks with SWIPT. IEEE Trans Wirel Commun, 2017, 16: 5644–5658
22 Zhou M X, Cui H Y, Song L Y, et al. Transmit-receive antenna pair selection in full duplex systems. IEEE Wirel Commun Lett, 2013, 3: 34–37
23 da Silva J M B, Ghauch H, Fodor G, et al. How to split UL/DL antennas in full-duplex cellular networks. In: Proceedings of IEEE International Conference on Communications Workshops (ICC Workshops), 2018. 1–6
24 Cela E. The Quadratic Assignment Problem: Theory and Algorithms, Volume 1. Berlin: Springer, 2013
25 Murray W, Ng K M. An algorithm for nonlinear optimization problems with binary variables. Comput Optim Appl, 2010, 47: 257–288
26 Rinaldi F. New results on the equivalence between zero-one programming and continuous concave programming. Optim Lett, 2009, 3: 377–386
27 Venkatraman G, Tolli A, Juntti M, et al. Multigroup multicast beamformer design for MISO-OFDM with antenna selection. IEEE Trans Signal Process, 2017, 65: 5832–5847
28 Melo W, Fampa M, Raupp F. Integrality gap minimization heuristics for binary mixed integer nonlinear programming. J Glob Optim, 2018, 71: 593–612
29 Lucidi S, Rinaldi F. Exact penalty functions for nonlinear integer programming problems. J Optim Theory Appl, 2010, 145: 479–488
30 Nguyen V D, Duong T Q, Tuan H D, et al. Spectral and energy efficiencies in full-duplex wireless information and power transfer. IEEE Trans Commun, 2017, 65: 2220–2233
31 Wiesel A, Eldar Y C, Shamai S. Linear precoding via conic optimization for fixed MIMO receivers. IEEE Trans Signal Process, 2005, 54: 161–176
32 Grant M, Boyd S. CVX: Matlab software for disciplined convex programming, version 2.1. 2014. http://cvxr.com/cvx/citing/
33 Boyd S, Vandenberghe L. Convex Optimization. Cambridge: Cambridge University Press, 2004
34 Peaucelle D, Henrion D, Labit Y, et al. User's guide for sedumi interface 1.04. 2002. https://homepages.laas.fr/henrion/papers/sdmguide.pdf
35 Nguyen H V, Nguyen V D, Dobre O A, et al. Joint power control and user association for NOMA-based full-duplex systems. IEEE Trans Commun, 2019, 67: 8037–8055